

Search for squarks and gluinos in events with jets and missing transverse energy in $p\bar{p}$ collisions at $\sqrt{s} = 1.96$ TeV

DØ Collaboration

V.M. Abazov^{an}, B. Abbott^{cd}, M. Abolins^{bt}, B.S. Acharya^{ag}, M. Adams^{bf}, T. Adams^{bd}, M. Agelou^u, J.-L. Agram^{v,w}, S.H. Ahn^{ai}, M. Ahsan^{bn}, G.D. Alexeev^{an}, G. Alkhazov^{ar}, A. Alton^{bs}, G. Alverson^{br}, G.A. Alves^b, M. Anastasoae^{am}, T. Andeen^{bh}, S. Anderson^{az}, B. Andrieu^t, M.S. Anzelc^{bh}, Y. Arnoud^q, M. Arov^{bg}, A. Askew^{bd}, B. Åsman^{as,at,au}, A.C.S. Assis Jesus^c, O. Atramentov^{bl}, C. Autermann^y, C. Avila^k, C. Ay^{ab}, F. Badaud^p, A. Baden^{bp}, L. Bagby^{bg}, B. Baldin^{be}, D.V. Bandurin^{an}, P. Banerjee^{ag}, S. Banerjee^{ag}, E. Barberis^{br}, P. Bargassa^{ci}, P. Baringer^{bm}, C. Barnes^{ax}, J. Barreto^b, J.F. Bartlett^{be}, U. Bassler^t, D. Bauer^{ax}, A. Bean^{bm}, M. Begalli^c, M. Begel^{bz}, C. Belanger-Champagne^{e,f,g,h}, A. Bellavance^{bv}, J.A. Benitez^{bt}, S.B. Beri^{ae}, G. Bernardi^t, R. Bernhard^{av}, L. Berntzon^r, I. Bertram^{aw}, M. Besançon^u, R. Beuselinck^{ax}, V.A. Bezzubov^{aq}, P.C. Bhat^{be}, V. Bhatnagar^{ae}, M. Binder^{ac}, C. Biscarat^{aw}, K.M. Black^{bq}, I. Blackler^{ax}, G. Blazey^{bg}, F. Blekman^{ax}, S. Blessing^{bd}, D. Bloch^{v,w}, K. Bloom^{bv}, U. Blumenschein^{aa}, A. Boehnlein^{be}, O. Boeriu^{bj}, T.A. Bolton^{bn}, F. Borchering^{be}, G. Borissov^{aw}, K. Bos^{al}, T. Bose^{cf}, A. Brandt^{cg}, R. Brock^{bt}, G. Brooijmans^{by}, A. Bross^{be}, D. Brown^{cg}, N.J. Buchanan^{bd}, D. Buchholz^{bh}, M. Buehler^{cj}, V. Buescher^{aa}, S. Burdin^{be}, S. Burke^{az}, T.H. Burnett^{ck}, E. Busato^t, C.P. Buszello^{ax}, J.M. Butler^{bq}, S. Calvet^r, J. Cammin^{bz}, S. Caron^{al}, W. Carvalho^c, B.C.K. Casey^{cf}, N.M. Cason^{bj}, H. Castilla-Valdez^{ak}, S. Chakrabarti^{ag}, D. Chakraborty^{bg}, K.M. Chan^{bz}, A. Chandra^{bc}, D. Chapin^{cf}, F. Charles^{v,w}, E. Cheu^{az}, F. Chevallier^q, D.K. Cho^{bq}, S. Choi^{aj}, B. Choudhary^{af}, L. Christofek^{bm}, D. Claes^{bv}, B. Clément^{v,w}, C. Clément^{as,at,au}, Y. Coadou^{e,f,g,h}, M. Cooke^{ci}, W.E. Cooper^{be}, D. Coppage^{bm}, M. Corcoran^{ci}, M.-C. Cousinou^r, B. Cox^{ay}, S. Crépe-Renaudin^q, D. Cutts^{cf}, M. Cwiok^{ah}, H. da Motta^b, A. Das^{bq}, M. Das^{bo}, B. Davies^{aw}, G. Davies^{ax}, G.A. Davis^{bh}, K. De^{cg}, P. de Jong^{al}, S.J. de Jong^{am}, E. De La Cruz-Burelo^{bs}, C. De Oliveira Martins^c, J.D. Degenhardt^{bs}, F. Déliot^u, M. Demarteau^{be}, R. Demina^{bz}, P. Demine^u, D. Denisov^{be}, S.P. Denisov^{aq}, S. Desai^{ca}, H.T. Diehl^{be}, M. Diesburg^{be}, M. Doidge^{aw}, A. Dominguez^{bv}, H. Dong^{ca}, L.V. Dudko^{ap}, L. Duflost^s, S.R. Dugad^{ag}, A. Duperrin^r, J. Dyer^{bt}, A. Dyshkant^{bg}, M. Eads^{bv}, D. Edmunds^{bt}, T. Edwards^{ay}, J. Ellison^{bc}, J. Elmsheuser^{ac}, V.D. Elvira^{be}, S. Eno^{bp}, P. Ermolov^{ap}, J. Estrada^{be}, H. Evans^{bi}, A. Evdokimov^{ao}, V.N. Evdokimov^{aq}, S.N. Fatakia^{bq}, L. Feligioni^{bq}, A.V. Ferapontov^{bn}, T. Ferbel^{bz}, F. Fiedler^{ac}, F. Filthaut^{am}, W. Fisher^{be}, H.E. Fisk^{be}, I. Fleck^{aa}, M. Ford^{ay}, M. Fortner^{bg}, H. Fox^{aa}, S. Fu^{be}, S. Fuess^{be}, T. Gadfort^{ck}, C.F. Galea^{am}, E. Gallas^{be}, E. Galyaev^{bj}, C. Garcia^{bz}, A. Garcia-Bellido^{ck}, J. Gardner^{bm}, V. Gavrilov^{ao}, A. Gay^{v,w}, P. Gay^p, D. Gelé^{v,w}, R. Gelhaus^{bc}, C.E. Gerber^{bf}, Y. Gershtein^{bd}, D. Gillberg^{e,f,g,h}, G. Ginther^{bz}, N. Gollub^{as,at,au}, B. Gómez^k, K. Gounder^{be}, A. Goussiou^{bj}, P.D. Grannis^{ca}, H. Greenlee^{be}, Z.D. Greenwood^{bo}, E.M. Gregores^d, G. Grenier^x, Ph. Gris^p, J.-F. Grivaz^s, S. Grünendahl^{be}, M.W. Grünewald^{ah}, F. Guo^{ca}, J. Guo^{ca}, G. Gutierrez^{be}

P. Gutierrez^{cd}, A. Haas^{by}, N.J. Hadley^{bp}, P. Haefner^{ac}, S. Hagopian^{bd}, J. Haley^{bw}, I. Hall^{cd},
 R.E. Hall^{bb}, L. Han^j, K. Hanagaki^{be}, K. Harder^{bn}, A. Harel^{bz}, R. Harrington^{br}, J.M. Hauptman^{bl},
 R. Hauser^{bt}, J. Hays^{bh}, T. Hebbeker^y, D. Hedin^{bg}, J.G. Hegeman^{al}, J.M. Heinmiller^{bf},
 A.P. Heinson^{bc}, U. Heintz^{bq}, C. Hensel^{bm}, G. Hesketh^{br}, M.D. Hildreth^{bj}, R. Hirosky^{cj},
 J.D. Hobbs^{ca}, B. Hoeneisen^o, M. Hohlfeld^s, S.J. Hong^{ai}, R. Hooper^{cf}, P. Houben^{al}, Y. Hu^{ca},
 V. Hynek^l, I. Iashvili^{bx}, R. Illingworth^{be}, A.S. Ito^{be}, S. Jabeen^{bq}, M. Jaffré^s, S. Jain^{cd}, K. Jakobs^{aa},
 C. Jarvis^{bp}, A. Jenkins^{ax}, R. Jesik^{ax}, K. Johns^{az}, C. Johnson^{by}, M. Johnson^{be}, A. Jonckheere^{be},
 P. Jonsson^{ax}, A. Juste^{be}, D. Käfer^y, S. Kahn^{cb}, E. Kajfasz^r, A.M. Kalinin^{an}, J.M. Kalk^{bo},
 J.R. Kalk^{bt}, S. Kappler^y, D. Karmanov^{ap}, J. Kasper^{bq}, I. Katsanos^{by}, D. Kau^{bd}, R. Kaur^{ae},
 R. Kehoe^{ch}, S. Kermiche^r, S. Kesisoglou^{cf}, A. Khanov^{ce}, A. Kharchilava^{bx}, Y.M. Kharzheev^{an},
 D. Khatidze^{by}, H. Kim^{cg}, T.J. Kim^{ai}, M.H. Kirby^{am}, B. Klima^{be}, J.M. Kohli^{ae}, J.-P. Konrath^{aa},
 M. Kopal^{cd}, V.M. Korablev^{aq}, J. Kotcher^{cb}, B. Kothari^{by}, A. Koubarovsky^{ap}, A.V. Kozelov^{aq},
 J. Kozminski^{bt}, A. Kryemadhi^{cj}, S. Krzywdzinski^{be}, T. Kuhl^{ab}, A. Kumar^{bx}, S. Kunori^{bp},
 A. Kupcoⁿ, T. Kurča^{x,1}, J. Kvita^l, S. Lager^{as,at,au}, S. Lammers^{by}, G. Landsberg^{cf}, J. Lazoflores^{bd},
 A.-C. Le Bihan^{v,w}, P. Lebrun^x, W.M. Lee^{bg}, A. Leflat^{ap}, F. Lehner^{av}, C. Leonidopoulos^{by},
 V. Lesne^p, J. Leveque^{az}, P. Lewis^{ax}, J. Li^{cg}, Q.Z. Li^{be}, J.G.R. Lima^{bg}, D. Lincoln^{be}, J. Linnemann^{bt},
 V.V. Lipaev^{aq}, R. Lipton^{be}, Z. Liu^{e,f,g,h}, L. Lobo^{ax}, A. Lobodenko^{ar}, M. Lokajicekⁿ, A. Lounis^{v,w},
 P. Love^{aw}, H.J. Lubatti^{ck}, M. Lynker^{bj}, A.L. Lyon^{be}, A.K.A. Maciel^b, R.J. Madaras^{ba}, P. Mättig^{ad},
 C. Magass^y, A. Magerkurth^{bs}, A.-M. Magnan^q, N. Makovec^s, P.K. Mal^{bj}, H.B. Malbouisson^c,
 S. Malik^{bv}, V.L. Malyshev^{an}, H.S. Maoⁱ, Y. Maravin^{bn}, M. Martens^{be}, S.E.K. Mattingly^{cf},
 R. McCarthy^{ca}, R. McCroskey^{az}, D. Meder^{ab}, A. Melnitchouk^{bu}, A. Mendes^r, L. Mendoza^k,
 M. Merkin^{ap}, K.W. Merritt^{be}, A. Meyer^y, J. Meyer^z, M. Michaut^u, H. Miettinen^{ci}, T. Millet^x,
 J. Mitrevski^{by}, J. Molina^c, N.K. Mondal^{ag}, J. Monk^{ay}, R.W. Moore^{e,f,g,h}, T. Moulik^{bm},
 G.S. Muanza^s, M. Mulders^{be}, M. Mulhearn^{by}, L. Mundim^c, Y.D. Mutaf^{ca}, E. Nagy^r,
 M. Naimuddin^{af}, M. Narain^{bq}, N.A. Naumann^{am}, H.A. Neal^{bs}, J.P. Negret^k, S. Nelson^{bd},
 P. Neustroev^{ar}, C. Noeding^{aa}, A. Nomerotski^{be}, S.F. Novaes^d, T. Nunnemann^{ac}, V. O'Dell^{be},
 D.C. O'Neil^{e,f,g,h}, G. Obrant^{ar}, V. Oguri^c, N. Oliveira^c, N. Oshima^{be}, R. Otec^m,
 G.J. Otero y Garzón^{bf}, M. Owen^{ay}, P. Padley^{ci}, N. Parashar^{bk}, S.-J. Park^{bz}, S.K. Park^{ai}, J. Parsons^{by},
 R. Partridge^{cf}, N. Parua^{ca}, A. Patwa^{cb}, G. Pawloski^{ci}, P.M. Perea^{bc}, E. Perez^u, K. Peters^{ay},
 P. Pétroff^s, M. Petteni^{ax}, R. Piegaiia^a, M.-A. Pleier^z, P.L.M. Podesta-Lerma^{ak}, V.M. Podstavkov^{be},
 Y. Pogorelov^{bj}, M.-E. Pol^b, A. Pompoš^{cd}, B.G. Pope^{bt}, A.V. Popov^{aq}, W.L. Prado da Silva^c,
 H.B. Prosper^{bd}, S. Protopopescu^{cb}, J. Qian^{bs}, A. Quadt^z, B. Quinn^{bu}, K.J. Rani^{ag}, K. Ranjan^{af},
 P.A. Rapidis^{be}, P.N. Ratoff^{aw}, P. Renkel^{ch}, S. Reucroft^{br}, M. Rijssenbeek^{ca}, I. Ripp-Baudot^{v,w},
 F. Rizatdinova^{ce}, S. Robinson^{ax}, R.F. Rodrigues^c, C. Royon^u, P. Rubinov^{be}, R. Ruchti^{bj}, V.I. Rud^{ap},
 G. Sajot^q, A. Sánchez-Hernández^{ak}, M.P. Sanders^{bp}, A. Santoro^c, G. Savage^{be}, L. Sawyer^{bo},
 T. Scanlon^{ax}, D. Schaile^{ac}, R.D. Schamberger^{ca}, Y. Scheglov^{ar}, H. Schellman^{bh},
 P. Schieferdecker^{ac}, C. Schmitt^{ad}, C. Schwanenberger^{ay}, A. Schwartzman^{bw}, R. Schwienhorst^{bt},
 S. Sengupta^{bd}, H. Severini^{cd}, E. Shabalina^{bf}, M. Shamim^{bn}, V. Shary^u, A.A. Shchukin^{aq},
 W.D. Shephard^{bj}, R.K. Shivpuri^{af}, D. Shpakov^{br}, V. Siccardi^{v,w}, R.A. Sidwell^{bn}, V. Simak^m,
 V. Sirotenko^{be}, P. Skubic^{cd}, P. Slattery^{bz}, R.P. Smith^{be}, G.R. Snow^{bv}, J. Snow^{cc}, S. Snyder^{cb},
 S. Söldner-Rembold^{ay}, X. Song^{bg}, L. Sonnenschein^t, A. Sopczak^{aw}, M. Sosebee^{cg}, K. Soustruznik^l,
 M. Souza^b, B. Spurlock^{cg}, J. Stark^q, J. Steele^{bo}, K. Stevenson^{bi}, V. Stolin^{ao}, A. Stone^{bf},
 D.A. Stoyanova^{aq}, J. Strandberg^{as,at,au}, M.A. Strang^{bx}, M. Strauss^{cd}, R. Ströhmer^{ac}, D. Strom^{bh},
 M. Strovink^{ba}, L. Stutte^{be}, S. Sumowidagdo^{bd}, A. Sznajder^c, M. Talby^r, P. Tamburello^{az},
 W. Taylor^{e,f,g,h}, P. Telford^{ay}, J. Temple^{az}, B. Tiller^{ac}, M. Titov^{aa}, V.V. Tokmenin^{an}, M. Tomoto^{be},

T. Toole^{bp}, I. Torchiani^{aa}, S. Towers^{aw}, T. Trefzger^{ab}, S. Trincaz-Duvoid^t, D. Tsybychev^{ca},
 B. Tuchming^u, C. Tully^{bw}, A.S. Turcot^{ay}, P.M. Tuts^{by}, R. Unalan^{bt}, L. Uvarov^{ar}, S. Uvarov^{ar},
 S. Uzunyan^{bg}, B. Vachon^{e,f,g,h}, P.J. van den Berg^{al}, R. Van Kooten^{bi}, W.M. van Leeuwen^{al},
 N. Varelas^{bf}, E.W. Varnes^{az}, A. Vartapetian^{cg}, I.A. Vasilyev^{aq}, M. Vaupel^{ad}, P. Verdier^{x,*},
 L.S. Vertogradov^{an}, M. Verzocchi^{bc}, F. Villeneuve-Seguiet^{ax}, P. Vint^{ax}, J.-R. Vlimant^t,
 E. Von Toerne^{bn}, M. Voutilainen^{bv,2}, M. Vreeswijk^{al}, H.D. Wahl^{bd}, L. Wang^{bp}, J. Warchol^{bj},
 G. Watts^{ck}, M. Wayne^{bj}, M. Weber^{bc}, H. Weerts^{bt}, N. Wermes^z, M. Wetstein^{bp}, A. White^{cg},
 D. Wicke^{ad}, G.W. Wilson^{bm}, S.J. Wimpenny^{bc}, M. Wobisch^{bc}, J. Womersley^{bc}, D.R. Wood^{br},
 T.R. Wyatt^{ay}, Y. Xie^{cf}, N. Xuan^{bj}, S. Yacoob^{bh}, R. Yamada^{bc}, M. Yan^{bp}, T. Yasuda^{bc},
 Y.A. Yatsunenkov^{an}, K. Yip^{cb}, H.D. Yoo^{cf}, S.W. Youn^{bh}, C. Yu^q, J. Yu^{cg}, A. Yurkewicz^{ca},
 A. Zatserklyaniy^{bg}, C. Zeitnitz^{ad}, D. Zhang^{bc}, T. Zhao^{ck}, Z. Zhao^{bs}, B. Zhou^{bs}, J. Zhu^{ca},
 M. Zielinski^{bz}, D. Zieminska^{bi}, A. Zieminski^{bi}, V. Zutshi^{bg}, E.G. Zverev^{ap}

^a Universidad de Buenos Aires, Buenos Aires, Argentina

^b LAFEX, Centro Brasileiro de Pesquisas Físicas, Rio de Janeiro, Brazil

^c Universidade do Estado do Rio de Janeiro, Rio de Janeiro, Brazil

^d Instituto de Física Teórica, Universidade Estadual Paulista, São Paulo, Brazil

^e University of Alberta, Edmonton, AB, Canada

^f Simon Fraser University, Burnaby, BC, Canada

^g York University, Toronto, ON, Canada

^h McGill University, Montreal, PQ, Canada

ⁱ Institute of High Energy Physics, Beijing, People's Republic of China

^j University of Science and Technology of China, Hefei, People's Republic of China

^k Universidad de los Andes, Bogotá, Colombia

^l Center for Particle Physics, Charles University, Prague, Czech Republic

^m Czech Technical University, Prague, Czech Republic

ⁿ Center for Particle Physics, Institute of Physics, Academy of Sciences of the Czech Republic, Prague, Czech Republic

^o Universidad San Francisco de Quito, Quito, Ecuador

^p Laboratoire de Physique Corpusculaire, IN2P3-CNRS, Université Blaise Pascal, Clermont-Ferrand, France

^q Laboratoire de Physique Subatomique et de Cosmologie, IN2P3-CNRS, Université de Grenoble 1, Grenoble, France

^r CPPM, IN2P3-CNRS, Université de la Méditerranée, Marseille, France

^s IN2P3-CNRS, Laboratoire de l'Accélérateur Linéaire, Orsay, France

^t LPNHE, IN2P3-CNRS, Universités Paris VI and VII, Paris, France

^u DAPNIA/Service de Physique des Particules, CEA, Saclay, France

^v IReS, IN2P3-CNRS, Université Louis Pasteur, Strasbourg, France

^w Université de Haute Alsace, Mulhouse, France

^x Institut de Physique Nucléaire de Lyon, IN2P3-CNRS, Université Claude Bernard, Villeurbanne, France

^y III. Physikalisches Institut A, RWTH Aachen, Aachen, Germany

^z Physikalisches Institut, Universität Bonn, Bonn, Germany

^{aa} Physikalisches Institut, Universität Freiburg, Freiburg, Germany

^{ab} Institut für Physik, Universität Mainz, Mainz, Germany

^{ac} Ludwig-Maximilians-Universität München, München, Germany

^{ad} Fachbereich Physik, University of Wuppertal, Wuppertal, Germany

^{ae} Panjab University, Chandigarh, India

^{af} Delhi University, Delhi, India

^{ag} Tata Institute of Fundamental Research, Mumbai, India

^{ah} University College Dublin, Dublin, Ireland

^{ai} Korea Detector Laboratory, Korea University, Seoul, South Korea

^{aj} SungKyunKwan University, Suwon, South Korea

^{ak} CINVESTAV, Mexico City, Mexico

^{al} FOM-Institute NIKHEF and University of Amsterdam/NIKHEF, Amsterdam, The Netherlands

^{am} Radboud University Nijmegen/NIKHEF, Nijmegen, The Netherlands

^{an} Joint Institute for Nuclear Research, Dubna, Russia

^{ao} Institute for Theoretical and Experimental Physics, Moscow, Russia

^{ap} Moscow State University, Moscow, Russia

^{aq} Institute for High Energy Physics, Protvino, Russia

^{ar} Petersburg Nuclear Physics Institute, St. Petersburg, Russia

^{as} Lund University, Lund, Sweden

^{at} Royal Institute of Technology and Stockholm University, Stockholm, Sweden

^{au} Uppsala University, Uppsala, Sweden

^{av} Physik Institut der Universität Zürich, Zürich, Switzerland

^{aw} Lancaster University, Lancaster, United Kingdom

- ^{ax} Imperial College, London, United Kingdom
^{ay} University of Manchester, Manchester, United Kingdom
^{az} University of Arizona, Tucson, AZ 85721, USA
^{ba} Lawrence Berkeley National Laboratory and University of California, Berkeley, CA 94720, USA
^{bb} California State University, Fresno, CA 93740, USA
^{bc} University of California, Riverside, CA 92521, USA
^{bd} Florida State University, Tallahassee, FL 32306, USA
^{be} Fermi National Accelerator Laboratory, Batavia, IL 60510, USA
^{bf} University of Illinois at Chicago, Chicago, IL 60607, USA
^{bg} Northern Illinois University, DeKalb, IL 60115, USA
^{bh} Northwestern University, Evanston, IL 60208, USA
^{bi} Indiana University, Bloomington, IN 47405, USA
^{bj} University of Notre Dame, Notre Dame, IN 46556, USA
^{bk} Purdue University Calumet, Hammond, IN 46323, USA
^{bl} Iowa State University, Ames, IA 50011, USA
^{bm} University of Kansas, Lawrence, KS 66045, USA
^{bn} Kansas State University, Manhattan, KS 66506, USA
^{bo} Louisiana Technical University, Ruston, LA 71272, USA
^{bp} University of Maryland, College Park, MD 20742, USA
^{bq} Boston University, Boston, MA 02215, USA
^{br} Northeastern University, Boston, MA 02115, USA
^{bs} University of Michigan, Ann Arbor, MI 48109, USA
^{bt} Michigan State University, East Lansing, MI 48824, USA
^{bu} University of Mississippi, University, MS 38677, USA
^{bv} University of Nebraska, Lincoln, NE 68588, USA
^{bw} Princeton University, Princeton, NJ 08544, USA
^{bx} State University of New York, Buffalo, NY 14260, USA
^{by} Columbia University, New York, NY 10027, USA
^{bz} University of Rochester, Rochester, NY 14627, USA
^{ca} State University of New York, Stony Brook, NY 11794, USA
^{cb} Brookhaven National Laboratory, Upton, NY 11973, USA
^{cc} Langston University, Langston, OK 73050, USA
^{cd} University of Oklahoma, Norman, OK 73019, USA
^{ce} Oklahoma State University, Stillwater, OK 74078, USA
^{cf} Brown University, Providence, RI 02912, USA
^{cg} University of Texas, Arlington, TX 76019, USA
^{ch} Southern Methodist University, Dallas, TX 75275, USA
^{ci} Rice University, Houston, TX 77005, USA
^{cj} University of Virginia, Charlottesville, VA 22901, USA
^{ck} University of Washington, Seattle, WA 98195, USA

Received 15 April 2006; received in revised form 12 May 2006; accepted 14 May 2006

Available online 24 May 2006

Editor: L. Rolandi

Abstract

The results of a search for squarks and gluinos using data from $p\bar{p}$ collisions recorded at a center-of-mass energy of 1.96 TeV by the DØ detector at the Fermilab Tevatron Collider are reported. The topologies analyzed consist of acoplanar-jet and multijet events with large missing transverse energy. No evidence for the production of squarks or gluinos was found in a data sample of 310 pb^{-1} . Lower limits of 325 and 241 GeV were derived at the 95% C.L. on the squark and gluino masses, respectively, within the framework of minimal supergravity with $\tan\beta = 3$, $A_0 = 0$, and $\mu < 0$.

© 2006 Elsevier B.V. All rights reserved.

PACS: 14.80.Ly; 12.60.Jv; 13.85.Rm

Supersymmetric models predict the existence of spin-0 quarks, or squarks (\tilde{q}), and spin-1/2 gluons, or gluinos (\tilde{g}),

as partners of the ordinary quarks and gluons. Supersymmetric particles carry a value of -1 for R -parity, a multiplicative quantum number, while $R = 1$ for standard model (SM) particles. If R -parity is conserved, as assumed in the following, supersymmetric particles are produced in pairs. Their decay leads to SM particles and to the lightest supersymmetric particle (LSP), which is stable. In supersymmetric models inspired

* Corresponding author.

E-mail address: verdier@ipnl.in2p3.fr (P. Verdier).

¹ On leave from IEP SAS Kosice, Slovakia.

² Visitor from Helsinki Institute of Physics, Helsinki, Finland.

by supergravity [1], the commonly accepted LSP candidate is the lightest neutralino ($\tilde{\chi}_1^0$, a mixture of the superpartners of the neutral gauge and Higgs bosons), which is weakly interacting, thus escaping detection and providing the classic missing transverse energy (\cancel{E}_T) signature at colliders. The most copiously produced supersymmetric particles in $p\bar{p}$ collisions should be, if sufficiently light, colored particles, i.e., squarks and gluinos. If squarks are lighter than gluinos, they will tend to decay according to $\tilde{q} \rightarrow q\tilde{\chi}_1^0$, and their pair production will yield an acoplanar-jet topology with \cancel{E}_T . If gluinos are lighter than squarks, their pair production and decay *via* $\tilde{g} \rightarrow q\bar{q}\tilde{\chi}_1^0$ will lead to topologies containing a large number of jets and \cancel{E}_T .

In this Letter, a search for squarks and gluinos in topologies with jets and large \cancel{E}_T is reported, using 310 pb^{-1} of data collected at a center-of-mass energy of 1.96 TeV with the DØ detector during Run II of the Fermilab Tevatron $p\bar{p}$ Collider. The search was conducted within the framework of the minimal supergravity model (mSUGRA) [1]. Previous direct mass limits are 195 GeV for gluinos if squarks are very heavy, and 300 GeV for squarks and gluinos of equal masses [2,3].

A detailed description of the DØ detector can be found in Ref. [4]. The central tracking system consists of a silicon microstrip tracker and a central fiber tracker, both located within a 2 T superconducting solenoidal magnet. A liquid-argon and uranium calorimeter covers pseudorapidities up to $|\eta| \approx 4.2$, where $\eta = -\ln[\tan(\theta/2)]$ and θ is the polar angle with respect to the proton beam direction. The calorimeter consists of three sections, housed in separate cryostats: the central one covers $|\eta| \lesssim 1.1$, and the two end sections extend the coverage to larger $|\eta|$. The calorimeter is segmented in depth, with four electromagnetic layers followed by up to five hadronic layers. It is also segmented in projective towers of size 0.1×0.1 in η - ϕ space, where ϕ is the azimuthal angle in radians. Calorimeter cells are defined as intersections of towers and layers. Additional sampling is provided by scintillating tiles in the regions at the boundary between cryostats. An outer muon system, covering $|\eta| < 2$, consists of a layer of tracking detectors and scintillation trigger counters in front of 1.8 T toroids, followed by two similar layers after the toroids. Jets are reconstructed from the energy deposited in calorimeter towers using the Run II cone algorithm [5] with radius $\mathcal{R} = \sqrt{(\Delta\phi)^2 + (\Delta\eta)^2} = 0.5$. The jet energy scale (JES) is derived from the transverse momentum balance in photon-plus-jet events. The \cancel{E}_T is calculated from all calorimeter cells, and corrected for the jet energy scale and for reconstructed muons.

The DØ trigger system consists of three levels, L1, L2, and L3. The events used in this analysis were recorded using a jet trigger requiring missing transverse energy calculated using the sum of the jet momenta ($\cancel{E}_T = |\sum_{\text{jets}} \vec{p}_T|$). At L1, events were required to have at least three calorimeter towers of size $\Delta\phi \times \Delta\eta = 0.2 \times 0.2$ with transverse energy E_T greater than 5 GeV. Events with a large imbalance in transverse momentum were then selected by requiring \cancel{E}_T to be greater than 20 GeV and 30 GeV at L2 and L3, respectively. In a small fraction of the data sample recorded at a higher instantaneous luminosity, the acoplanarity, defined as the azimuthal angle between the two leading jets, was re-

quired to be less than 168.75° and 170° at L2 and L3, respectively.

The signal consists of jets and \cancel{E}_T . This topology also arises from SM processes with real \cancel{E}_T , such as $p\bar{p} \rightarrow Z + \text{jets}$ with $Z \rightarrow \nu\bar{\nu}$, and from multijet production when one or more jets are mismeasured (QCD background). Simulated events from SM and mSUGRA processes were produced using Monte Carlo (MC) generators, subjected to a full GEANT-based [6] simulation of the detector geometry and response, and processed through the same reconstruction chain as the data. The CTEQ5L [7] parton density functions (PDF) were used, and a Poisson-average of 0.8 minimum bias events was overlaid on each simulated event. The QCD background was not simulated, but estimated directly from data. To simulate $W/Z + \text{jets}$ and $t\bar{t}$ production, the ALPGEN 1.3 generator [8] was used, interfaced with PYTHIA 6.202 [9] for the simulation of initial and final state radiation and of jet hadronization. The next-to-leading order (NLO) cross sections were computed with MCFM 3.4.4 [10], or taken from Ref. [11] for $t\bar{t}$ production.

Squark and gluino production and decay were simulated with PYTHIA. The masses and couplings of the supersymmetric particles were calculated with ISAJET 7.58 [12] from the set of five mSUGRA parameters: m_0 and $m_{1/2}$, which are universal scalar and gaugino masses, and A_0 , a universal trilinear coupling, all defined at the scale of grand unification; $\tan\beta$, the ratio of the vacuum expectation values of the two Higgs fields; and the sign of the Higgs-mixing mass parameter μ . To retain consistency with earlier analyses [2,3], the following parameters were fixed: $A_0 = 0$, $\tan\beta = 3$, and $\mu < 0$. For the same reason, the production of scalar top quarks, or stops, was ignored. In the following, “squark mass” stands for the average mass of all squarks other than stops. All squark and gluino decay modes were taken into account in the simulation, including cascade decays such as $\tilde{g} \rightarrow q\bar{q}\tilde{\chi}_2^0$ with $\tilde{\chi}_2^0 \rightarrow \ell^+\ell^-\tilde{\chi}_1^0$. The NLO cross sections of the various signal processes were calculated with PROSPINO 2 [13].

Three benchmark scenarios have been considered. At low m_0 , the gluino is heavier than the squarks, and the process with the dominant cross section is $\tilde{q}\bar{q}$ production. A “dijet” analysis was optimized to search for events containing a pair of acoplanar jets. At high m_0 , the squarks are much heavier than the gluino, and the process with the highest cross section is therefore $\tilde{g}\bar{g}$ production. A “gluino” analysis was optimized to search for multijet events (≥ 4 jets). In the intermediate m_0 region, all squark–gluino production processes contribute to the total cross section, in particular the $\tilde{q}\bar{g}$ process becomes relevant. A “3-jets” analysis was optimized to search for events with at least three jets. The benchmark for this analysis is the case where $m_{\tilde{q}} = m_{\tilde{g}}$.

A common event preselection was used for the three analyses to select events with at least two jets and substantial \cancel{E}_T (≥ 40 GeV). The acoplanarity was required to be below 165° . The longitudinal position of the primary vertex with respect to the detector center was restricted, $|z| < 60$ cm, to ensure an efficient primary vertex reconstruction. The two leading jets, i.e., those with the largest transverse energies, were required to be in the central region of the calorimeter, $|\eta_{\text{det}}| < 0.8$, where

Table 1
Selection criteria for the three analyses (all energies in GeV); see the text for further details

Preselection cut	All analyses		
\cancel{E}_T	≥ 40		
Acoplanarity Vertex z pos.]	$< 165^\circ$ < 60 cm		
Selection cut	“dijet”	“3-jets”	“gluino”
1st jet E_T ¹	≥ 60	≥ 60	≥ 60
2nd jet E_T ¹	≥ 50	≥ 40	≥ 40
3rd jet E_T ¹	–	≥ 30	≥ 30
4th jet E_T ¹	–	–	≥ 20
Electron veto	yes	yes	yes
Muon veto	yes	yes	yes
$\Delta\phi(\cancel{E}_T, \text{jet}_1)$	$\geq 90^\circ$	$\geq 90^\circ$	$\geq 90^\circ$
$\Delta\phi(\cancel{E}_T, \text{jet}_2)$	$\geq 50^\circ$	$\geq 50^\circ$	$\geq 50^\circ$
$\Delta\phi_{\min}(\cancel{E}_T, \text{any jet})$	$\geq 40^\circ$	–	–
H_T	≥ 275	≥ 350	≥ 225
\cancel{E}_T	≥ 175	≥ 100	≥ 75

¹ Jets subject to an E_T cut are also required to be central ($|\eta_{\text{det}}| < 0.8$), with an electromagnetic fraction below 0.95, and to have CPF ≥ 0.05 .

η_{det} is the jet pseudorapidity calculated under the assumption that the jet originates from the detector center. These jets must have their fraction of energy in the electromagnetic layers of the calorimeter smaller than 0.95. Minimum transverse energies of 60 and 40 GeV were required for the first and second leading jets, respectively.

The tracking capabilities of the Run II DØ detector were used to significantly reduce the QCD background. A comparison of the jet energy with the energy carried by its associated charged particles was performed. In particular, the ratio CPF of the transverse momentum carried by tracks associated with the jet to the jet E_T is expected to be close to zero if an incorrect primary vertex was selected. The two leading jets were required to have CPF larger than 0.05.

Different selection criteria were next applied in the three analyses, as summarized in Table 1. In the “dijet” analysis, the cut on the second jet E_T was raised to 50 GeV. In the “3-jets” and “gluino” analyses, a third and fourth jet were required, respectively. They must fulfill the same quality criteria as the two leading jets, except for the E_T cuts which were set at 30 and 20 GeV. In all three analyses, a veto on isolated electrons or muons with $p_T > 10$ GeV rejects a large fraction of events originating from the $W/Z + \text{jets}$ processes. The azimuthal angles between the \cancel{E}_T and the first jet, $\Delta\phi(\cancel{E}_T, \text{jet}_1)$, and the second jet, $\Delta\phi(\cancel{E}_T, \text{jet}_2)$, were used to remove events where the energy of one jet was mismeasured, generating \cancel{E}_T aligned with that jet. The cuts are $\Delta\phi(\cancel{E}_T, \text{jet}_1) \geq 90^\circ$ and $\Delta\phi(\cancel{E}_T, \text{jet}_2) \geq 50^\circ$.

In the “dijet” analysis, QCD events were further suppressed by requiring that the minimum azimuthal angle $\Delta\phi_{\min}(\cancel{E}_T, \text{any jet})$ between the \cancel{E}_T and any jet with $E_T > 15$ GeV be greater than 40° . Because of the higher jet multiplicity, this criterion was not used in the “3-jets” and “gluino” analyses.

The “dijet” $\Delta\phi_{\min}(\cancel{E}_T, \text{any jet})$ cut along with the two final cuts on $H_T = \sum_{\text{jets}} E_T$ and on \cancel{E}_T were optimized by minimizing the expected upper limit on the cross section in the absence of signal. To this end, as well as for the derivation of the final results, the modified frequentest CL_s method [14] was used. For each set of cuts tested, the QCD background contribution was estimated from an exponential fit to the \cancel{E}_T distribution below 60 GeV, after subtraction of the SM background processes, extrapolated above the chosen \cancel{E}_T cut value. The optimal cuts thus determined are given in Table 1 for the three analyses. Fig. 1 shows: the $\Delta\phi_{\min}(\cancel{E}_T, \text{any jet})$ distribution after applying the “dijet” analysis criteria with a \cancel{E}_T cut reduced to 80 GeV and without requiring the conditions on $\Delta\phi_{\min}(\cancel{E}_T, \text{any jet})$ itself and on $\Delta\phi(\cancel{E}_T, \text{jet}_2)$; the H_T distribution after applying all the “3-jets” analysis criteria except the one on H_T ; and the \cancel{E}_T distribution after applying all the “gluino” analysis criteria except the one on \cancel{E}_T .

The numbers of events selected by each analysis are reported in Table 2, as well as the numbers of background events expected. Six events were selected by the “dijet” analysis, four by the “3-jets” analysis, and ten by the “gluino” analysis. The total expected background contributions are 4.8, 3.9 and 10.3 events, respectively. The main background contributions are from $Z \rightarrow \nu\bar{\nu} + \text{jets}$, $W \rightarrow l\nu + \text{jets}$, and $t\bar{t} \rightarrow b\bar{b} q\bar{q}'l\nu$. The QCD background was evaluated from a fit to the \cancel{E}_T distribution as described above. It was found to be negligible in the “dijet” and “3-jets” analyses, and was therefore conservatively ignored. A QCD contribution of $0.7^{+0.7}_{-0.4}$ event was estimated in the “gluino” analysis. The uncertainties were obtained by taking into account the accuracy of the fit parameter determination and by varying the range of the fit. The signal efficiencies are given in Table 2 for the three benchmark scenarios, with the corresponding values of m_0 , $m_{1/2}$, the squark and gluino masses, and the NLO cross section. The quoted systematic uncertainties are discussed below.

The uncertainty coming from the JES corrections is one of the most important. It is typically of the order of 13% for the SM backgrounds and 10% for the signal efficiencies. The uncertainties on the jet energy resolution, on the jet track confirmation, and on the jet reconstruction and identification efficiencies were evaluated. They lead to systematic uncertainties of 3.5%, 4.0% and 5.4% in the “dijet,” “3-jets,” and “gluino” analyses, respectively. The trigger was found to be fully efficient for the event samples surviving all analysis cuts. Conservatively, a 2% uncertainty was set on the trigger efficiency. The uncertainty on the determination of the luminosity is 6.5% [15]. All of these uncertainties are fully correlated between signal and SM backgrounds. A 15% systematic uncertainty was set on the $W/Z + \text{jets}$ and $t\bar{t}$ NLO cross sections. The uncertainty on the signal acceptance due to the PDF choice was determined to be 6%, using the forty-eigenvector basis of the CTEQ6.1M PDF set [16].

The signal cross sections are very sensitive to the PDF choice and to the renormalization and factorization scale, μ_{rf} . The nominal NLO cross sections, σ_{nom} , were computed with the CTEQ6.1M PDF and for $\mu_{\text{rf}} = Q$, where Q was taken to be equal to $m_{\tilde{g}}$ for $\tilde{g}\tilde{g}$ production, $m_{\tilde{q}}$ for $\tilde{q}\tilde{q}$ and $\tilde{q}\tilde{q}'$ pro-

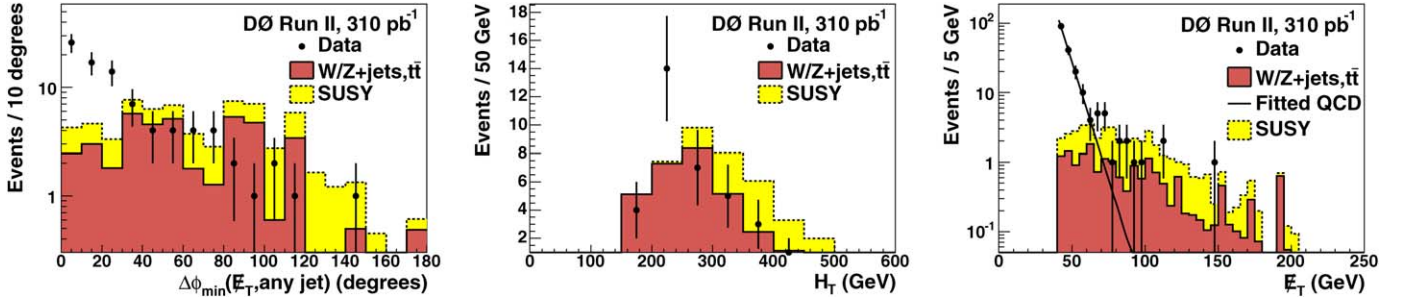


Fig. 1. $\Delta\phi_{\min}(\cancel{E}_T, \text{any jet})$ distribution after applying the “dijet” analysis criteria with a \cancel{E}_T cut reduced to 80 GeV and without requiring the conditions on $\Delta\phi_{\min}(\cancel{E}_T, \text{any jet})$ itself and on $\Delta\phi(\cancel{E}_T, \text{jet}_2)$ (left), H_T distribution after applying all the “3-jets” analysis criteria except the one on H_T (middle), and \cancel{E}_T distribution after applying all the “gluino” analysis criteria except the final one on \cancel{E}_T (right), for data (points with error bars), for non-QCD SM background (full histogram), and for signal MC (dashed histogram on top of SM). For each analysis, the signal drawn is the one for the appropriate benchmark scenario (Table 2). In the \cancel{E}_T distribution, the fitted QCD background is also drawn.

Table 2

For each analysis, information on the signal for which it was optimized: m_0 , $m_{1/2}$, $m_{\tilde{g}}$, $m_{\tilde{q}}$ and nominal NLO cross section, signal efficiency, the number of events observed, the number of events expected from SM and QCD backgrounds and the 95% C.L. signal cross section upper limit. The first uncertainty is statistical and the second is systematic

Analysis	$(m_0, m_{1/2})$ (GeV)	$(m_{\tilde{g}}, m_{\tilde{q}})$ (GeV)	σ_{nom} (pb)	$\epsilon_{\text{sig.}}$ (%)	$N_{\text{Obs.}}$	$N_{\text{backgrd.}}$	σ_{95} (pb)
“dijet”	(25, 145)	(366, 318)	0.63	$6.2 \pm 0.4^{+1.1}_{-0.9}$	6	$4.8^{+4.4+1.1}_{-2.0-0.8}$	0.44
“3-jets”	(191, 126)	(330, 330)	0.64	$4.7 \pm 0.3^{+0.8}_{-0.7}$	4	$3.9^{+1.3+0.7}_{-1.0-0.8}$	0.45
“gluino”	(500, 80)	(240, 507)	2.41	$2.3 \pm 0.2^{+0.4}_{-0.3}$	10	$10.3^{+1.5+1.9}_{-1.4-2.5}$	1.72

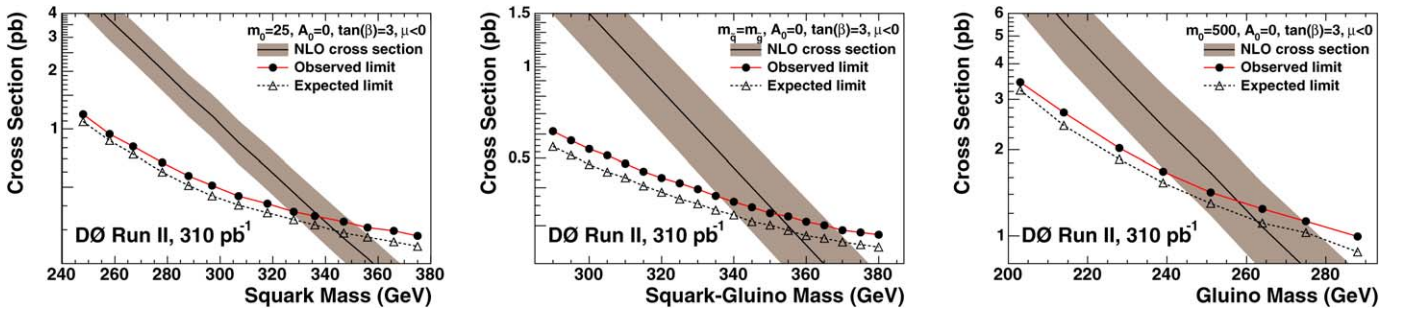


Fig. 2. For $\tan\beta = 3$, $A_0 = 0$, $\mu < 0$, observed (closed circles) and expected (open triangles) 95% C.L. upper limits on squark–gluino production cross sections combining the analyses for $m_0 = 25$ GeV (left), $m_{\tilde{q}} = m_{\tilde{g}}$ (middle), and $m_0 = 500$ GeV (right). The nominal production cross sections are also shown, with shaded bands corresponding to the PDF and renormalization-and-factorization scale uncertainties.

ductions, and $(m_{\tilde{q}} + m_{\tilde{g}})/2$ for $\tilde{q}\tilde{g}$ production. The uncertainty due to the choice of PDF was determined using the full set of CTEQ6.1M eigenvectors, with the individual uncertainties added in quadrature. The effect on the nominal signal cross sections, which varies between 15% and 50%, is dominated by the large uncertainty on the gluon distribution at high x . The effect of the renormalization and factorization scale was studied by calculating the signal cross sections for $\mu_{\text{rf}} = Q$, $\mu_{\text{rf}} = Q/2$ and $\mu_{\text{rf}} = 2 \times Q$. The factor two on this scale reduces or increases the nominal signal cross sections by 15–20%. The PDF and μ_{rf} effects were added in quadrature to compute minimum, σ_{min} , and maximum, σ_{max} , signal cross sections.

No significant excess of events was observed in the data with respect to the SM background expectation in any of the three analyses. Therefore, an excluded domain in the gluino–squark mass plane was determined as follows. The three analyses were

run over signal MC samples generated in the gluino–squark mass plane to compute signal efficiencies. Then, to take advantage of the different features of the three analyses, they were combined in the limit computation, with the small overlaps taken into account. In the data, no events were selected by more than one analysis.

Limits at the 95% C.L. were computed for three hypotheses on the signal cross sections: nominal, minimum, and maximum. Fig. 2 shows the observed and expected upper limits on squark–gluino production cross sections for the three benchmark scenarios. For the “3-jets” and “gluino” analyses, the expected limits computed with the numbers of events reported in Table 2 are almost identical to the observed ones. Once the combination of analyses is performed, the expected limits become slightly better than the observed limits at large m_0 and for $m_{\tilde{q}} = m_{\tilde{g}}$, as can be seen in Fig. 2.

Table 3

Absolute lower limits at the 95% C.L. on the squark and gluino masses (in GeV) as a function of the choice of signal cross section hypothesis as defined in the text. Numbers in parentheses correspond to the expected limits. These limits are valid for the mSUGRA parameters: $\tan\beta = 3$, $A_0 = 0$, $\mu < 0$

Hypothesis	Gluino mass	Squark mass
σ_{\min}	241 (246)	325 (330)
σ_{nom}	257 (261)	339 (344)
σ_{\max}	274 (280)	352 (358)

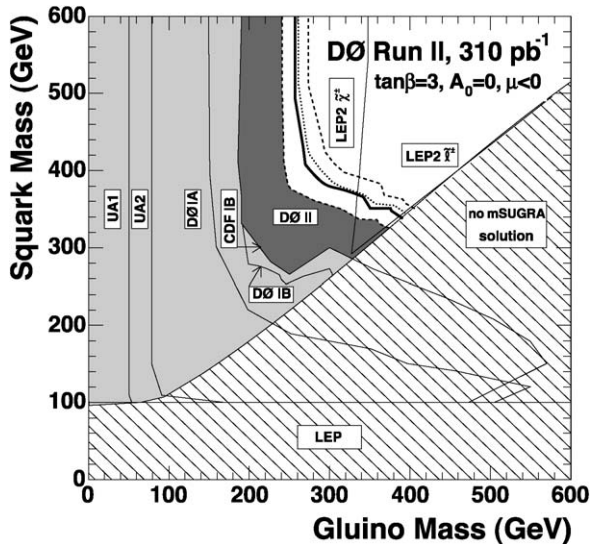


Fig. 3. In the gluino and squark mass plane, excluded regions at the 95% C.L. by direct searches in the mSUGRA framework with $\tan\beta = 3$, $A_0 = 0$, $\mu < 0$. The new region excluded by this analysis in the most conservative hypothesis (σ_{\min}) is shown in dark shading. The thick line is the limit of the excluded region for the σ_{nom} hypothesis. The corresponding expected limit is the dotted line. The band delimited by the two dashed lines shows the effect of the PDF choice and of a variation of μ_{rf} by a factor of two. Regions excluded by previous experiments are indicated in light shading [2,3,17]. The two thin lines indicate the indirect limits inferred from the LEP2 chargino and slepton searches [18]. The region where no mSUGRA solution can be found is shown hatched.

Fig. 3 shows the excluded domain in the gluino–squark mass plane. The absolute lower limits on the squark and gluino masses obtained in the most conservative hypothesis, σ_{\min} , are 325 and 241 GeV, respectively. The corresponding expected limits are 330 and 246 GeV. Table 3 summarizes these absolute limits as a function of the signal cross section hypothesis. Limits were also derived for the particular case $m_{\tilde{q}} = m_{\tilde{g}}$. For σ_{\min} , squark and gluino masses below 337 GeV are excluded, while the expected limit is 340 GeV. The observed limit becomes 351 GeV for σ_{nom} , and 368 GeV for σ_{\max} .

These results improve on the previous direct limits on squark and gluino masses [2,3,17]. They were obtained within the mSUGRA framework with $\tan\beta = 3$, $A_0 = 0$, and $\mu < 0$. A general scan of the mSUGRA parameter space is beyond the scope of the current analysis, but it has been verified that similar results would be obtained for a large class of parameter sets. The limits obtained at LEP on the chargino ($\tilde{\chi}^{\pm}$) and slepton ($\tilde{\ell}$) masses can be turned into constraints on the mSUGRA parameters m_0 and $m_{1/2}$ [18], and hence on the squark and gluino masses as shown in Fig. 3. The limits from Higgs bo-

son searches at LEP are even more constraining [18], actually ruling out all of the squark and gluino mass domain to which the Tevatron could be sensitive. The interpretation of these indirect constraints is however more sensitive to the details of the model considered than the direct limits presented here.

In summary, a search for events with jets and large \cancel{E}_T has been performed in a 310 pb^{-1} data sample from $p\bar{p}$ collisions at 1.96 TeV, collected by the DØ detector. Three analyses were designed, specifically targeted to the dijet, three-jet, and multi-jet topologies. The numbers of events observed are in agreement with the SM background predictions. The results have been interpreted in the framework of minimal supergravity with $\tan\beta = 3$, $A_0 = 0$, $\mu < 0$. For the central choice of PDF, and for a renormalization and factorization scale equal to the mass of the squark or gluino produced, the lower limits on the squark and gluino masses are 339 and 257 GeV at the 95% C.L. Taking into account the PDF uncertainties and allowing for a factor of two in the choice of scale, these limits are reduced to 325 and 241 GeV, respectively. These are the most constraining direct limits on the squark and gluino masses to date.

Acknowledgements

We thank the staffs at Fermilab and collaborating institutions, and acknowledge support from the DOE and NSF (USA); CEA and CNRS/IN2P3 (France); FASI, Rosatom and RFBR (Russia); CAPES, CNPq, FAPERJ, FAPESP and FUN-DUNESP (Brazil); DAE and DST (India); Colciencias (Colombia); CONACyT (Mexico); KRF and KOSEF (Korea); CON-ICET and UBACyT (Argentina); FOM (The Netherlands); PPARC (United Kingdom); MSMT (Czech Republic); CRC Program, CFI, NSERC and WestGrid Project (Canada); BMBF and DFG (Germany); SFI (Ireland); The Swedish Research Council (Sweden); Research Corporation; Alexander von Humboldt Foundation; and the Marie Curie Program.

References

- [1] H.P. Nilles, Phys. Rep. 110 (1984) 1.
- [2] DØ Collaboration, B. Abbott, et al., Phys. Rev. Lett. 83 (1999) 4937.
- [3] CDF Collaboration, T. Affolder, et al., Phys. Rev. Lett. 88 (2002) 041801.
- [4] DØ Collaboration, V.M. Abazov, et al., physics/0507191, Nucl. Instrum. Methods Phys. Res. A, submitted for publication.
- [5] G.C. Blazey, et al., in: U. Baur, R.K. Ellis, D. Zeppenfeld (Eds.), Proceedings of the Workshop: QCD and Weak Boson Physics in Run II, Fermilab, Batavia, IL, 2000, p. 47, see Section 3.5 for details.
- [6] R. Brun, F. Carminati, CERN Program Library Long Writeup W5013, 1993, unpublished.
- [7] H.L. Lai, et al., Eur. Phys. J. C 12 (2000) 375.
- [8] M.L. Mangano, et al., JHEP 0307 (2003) 001.
- [9] T. Sjöstrand, et al., Comput. Phys. Commun. 135 (2001) 238.
- [10] J.M. Campbell, R.K. Ellis, Phys. Rev. D 60 (1999) 113006.
- [11] N. Kidonakis, R. Vogt, Int. J. Mod. Phys. A 20 (2005) 3171.
- [12] F.E. Paige, S.D. Protopopescu, H. Baer, X. Tata, hep-ph/0312045.
- [13] W. Beenakker, R. Hopker, M. Spira, P.M. Zerwas, Nucl. Phys. B 492 (1997) 51.
- [14] T. Junk, Nucl. Instrum. Methods Phys. Res. A 434 (1999) 435; A. Read, in: 1st Workshop on Confidence Limits, CERN Report No. CERN-2000-005, 2000.
- [15] T. Edwards, et al., FERMILAB-TM-2278-E, 2004.

- [16] J. Pumplin, et al., JHEP 0207 (2002) 012;
D. Stump, et al., JHEP 0310 (2003) 046.
- [17] UA1 Collaboration, C. Albajar, et al., Phys. Lett. B 198 (1987) 261;
UA2 Collaboration, J. Alitti, et al., Phys. Lett. B 235 (1990) 363;
DØ Collaboration, S. Abachi, et al., Phys. Rev. Lett. 75 (1995) 618;
ALEPH Collaboration, A. Heister, et al., Phys. Lett. B 537 (2002) 5;
L3 Collaboration, P. Achard, et al., Phys. Lett. B 580 (2004) 37.
- [18] LEPSUSYWG, ALEPH, DELPHI, L3, OPAL Collaborations, note
LEPSUSYWG/02-06.2, <http://lepsusy.web.cern.ch/lepsusy/>.